BROADBAND ELECTRICALLY SHORT TRANSMITTERS VIA TIME-VARYING ANTENNA PROPERTIES

A Dissertation
Presented to
The Academic Faculty

By

Lee A. Thompson

In Partial Fulfillment
of the Requirements for the Master's
Degree in the
School of Electrical and Computer Engineering

Georgia Institute of Technology

December 2017

BROADBAND ELECTRICALLY SHORT TRANSMITTERS VIA TIME-VARYING ANTENNA PROPERTIES

Approved by:

Dr. Morris Cohen, Advisor
School of Electrical and Computer Engineering
Georgia Institute of Technology

Dr. Greg Durgin
School of Electrical and Computer Engineering
Georgia Institute of Technology

Dr. Andrew Peterson
School of Electrical and Computer Engineering
Georgia Institute of Technology

Date Approved: December 1, 2017

In loving memory of my late stepfather, Rendy L. Boland

ACKNOWLEDGEMENTS

I would like to thank Dr. Morris Cohen for mentoring and advising me over the past few years. At a school with the largest electrical and computer engineering program in the country, Dr. Cohen took the time to invest in me and help me succeed. It has been the highlight of my experience at Georgia Tech to work in the Low Frequency Radio Lab with Dr. Cohen. I will always look back on my years as a graduate student fondly because of this.

I would like to express a tremendous amount of gratitude to Dr. Greg Durgin and Dr. Andrew Peterson for being on my thesis advising committee. Thank you for taking the time to review my work. I realize that this is not a simple task.

Lastly, I would like to thank my friends and family for their continued support over the years. When circumstances seemed impossible and I was full of doubt, they were always there to remind me of who I am and what I wanted for myself.

Some of the underlying ideas in this work are covered under a pending patent PCT/US15/41725, entitled ”Electrically short antennas with enhanced radiation resistance”. This work has been supported by the Defense Advanced Research Projects Agency (DARPA).

TABLE OF CONTENTS

LIST OF TABLES

LIST OF FIGURES

SUMMARY

This thesis presents a theory by which an electrically short antenna can far exceed the Chu-Harrington limit through time-variant properties. This thesis details the design and implementation of the novel antenna, as well as experimental results gathered from its operation. Comparisons are made to conventional antennas, and the distinctions are based in a literature survey. Current issues with the antenna system are given, and suggestions for future work are included in the conclusion.

CHAPTER 1
INTRODUCTION AND BACKGROUND

The 21st century is commonly referred to as "The Information Age" by historians and the like due to the ease of accessing information digitally. Advances in radio and wireless technologies have shaped society by producing a convenient and ubiquitous information flow from sensors, cell phones, vehicles, and more. For all applications where such a wireless communication system is needed, size constraints play an important role in system design. While wireless communication systems may seem unrelated to system size in many applications, they are in fact a critical detail in others.

Physical size constraints most directly impact antenna performance in wireless communications systems. Antenna design is most commonly done when the length of the antenna is comparable to the wavelength. Antennas for which the size is substantially smaller are known as "electrically small", and provide far less bandwidth. Some may argue that the frequencies most consumable electronics operate at (approximately 2.4 GHz) are not prone to size constraints since the wavelength in air or free space is a meager 12 centimeters. Yet, there are applications when even this size is far too large, for example with wearable devices, or inside integrated circuits.

The Ultra High Frequency (UHF, 300 MHz$-$3 GHz) radio band is commonly used for high data rate communication systems due to the bandwidth available at these frequencies [1]. However, the content found in [1] addresses the fact that UHF band radio links typically require line-of-sight operation, and suffer from the effects of multipath and scattering. These properties, along with many others, make the UHF radio band untenable for any long range or even global wireless applications, such as global communications systems.

The pitfalls of the UHF radio band are precisely the strengths in the Very Low Frequency (VLF, 3$-$30 kHz) and Low Frequency (LF, 30$-$300 kHz) radio bands, where radio

signals can be received around the globe due to efficient reflection from the ionosphere between $60-90$ km altitude [2]. VLF/LF radio signals and lower radio bands experience extremely low loss as they propagate, as low as a few dB per 1000 km [3]. Another novel property of the VLF/LF radio band and those below it is the penetration into good conductors, such as sea water, due to the phenomena known as the skin effect. For this reason, VLF and LF radio broadcasts are currently a primary method for communication with submerged submarines, and also comprised two global navigation systems (Omega and LORAN-C) that existed well before the rise of the Global Positioning System [4], [5].

The VLF/LF waves are relatively easy to detect [6], and the propagation physics are fairly well understood in principle [7], but what has long been the struggle is pursuit of efficient transmission of these radio signals. The wavelength at such frequencies is on the order of kilometers. The electrically small antenna is the typically the only type of antenna realizable in these applications.

1.1 The Electrically Small Antenna

Existing theory on linear, time-invariant (LTI) antennas asserts that the physical volume that such an antenna occupies dictates its bandwidth, as shown seminally by Chu [8] and Harrington [9]. Furthermore, the relationship between bandwidth and gain in LTI antennas is established in [8] and [9], and is found to be constant for antennas with a dimension larger than r_o. This document is concerned with antennas in size below the aforementioned threshold, where the gain-bandwidth ratio exhibits a linear dependence with antenna size. The Chu-Harrington limit is succintly written as

$$Q \geq \frac{1}{(ka)^3} + \frac{1}{ka} \tag{1.1}$$

where

$$Q = \frac{f_c}{\Delta f}$$

and

$$k = \frac{2\pi f}{c}$$

The variable *a* is the radius of the smallest sphere which encapsulates the antenna. The wavenumber relates the frequency and medium to the wavelength. For applications related to this paper, consider a 3 meter source radiating at 30kHz in free space. Based off of the above theory,

$$a = 3m$$

$$k = \frac{2\pi(30000)}{c}$$

$$Q \geq 1.49 \times 10^8$$

For a center frequency of 30kHz, the limit predicts that the antenna will only have a bandwidth of 0.2mHz.

An antenna is commonly considered to be electrically small if its largest dimension does not exceed one-eighth of the wavelength [10]. Electrically small antennas (henceforth denoted as ESAs) are notorious for the tremendous amount of reactance associated with their input impedance, due to energy being stored in the near field. ESAs are of particular importance in the High Frequency (HF, $3-30$ MHz) band and lower frequency bands, as wavelength sized conductors for these frequencies are difficult to realize structurally.

1.2 Using the Electrically Small Antenna in Practice

Due to the large, reactive input impedance of ESAs, impedance matching the antenna to a feed can be difficult at best, and futile at worst. Relevant work was done in 1948 by Fano

[11] which established the theoretical limits on broadband impedance matching. Modern computing has built on the theory proposed in [11] to allow designers to compute a truly optimum solution to the Bode-Fano criterion and compare operational bandwidth tradeoffs in matching network design through H^{∞} functions [12]. These matching networks still face the theoretical bandwidth limits of the Bode-Fano criterion. Developments in negative impedance converters have led to non-foster impedance matching techniques, which utilize negative capacitances and inductances to achieve a wideband match to loads such as an electrically short antenna [13].

Others have developed theory instead on the structural characteristics of ESAs, as seen in [10], where electrically small half-wave wound conductor structures perform comparably to monopoles with ground planes considered to be electrically large. Ziolkowski et al. have suggested that efficient electrically small antennas may be realized through metamaterials, in which a double negative material is used as a shell around a traditional conductor [14]. The simulated increase in radiated power is in excess of 60dB at some frequencies, however, the standalone structure is resonant at particular frequencies and thus not truly broadband.

Recent advances in microelectronics have enabled techniques such as Direct Antenna Modulation (DAM), in which an RF switch is used to vary the resonant frequency of an electrically small antenna [15]. These authors reported more than a 13x improvement in bandwidth using this technique. The same technological advances in RF switching technology that enabled DAM will prove to be relevant to the antenna system featured in this document. All of these efforts, however, are essentially engineering management of the same fundamental issue first laid out by Chu and Harrington, that an electrically small antenna will face a fundamental tradeoff between efficiency and bandwidth. It is our contention through the rest of this thesis that this tradeoff can be entirely removed altogether. We present both theory and a real demonstration showing this to be true. We should note, however, that our results here do not in any way refute or break the long-revered Chu-

Harrington limit. Rather, we call attention to the fact that Chu-Harrington assumes a time-invariant antenna, and it is this assumption that we will break in order to circumvent the ordinary efficiency-bandwidth tradeoff entirely.

1.3 Existing VLF Antennas

Most VLF transmitters are operated by navies around the world for communication with undersea submarines. These transmitters employ tremendous monopole antennas in order to radiate. Since the wavelength at VLF in free space at the least is a kilometer, even these antennas are electrically small. Top-loading is commonly used to increase the capacitance of such an antenna, and effectively transforms a monopole into an umbrella antenna with guy wires. A series inductor is then used to achieve resonance. This information and more can be found in [16].

Others have searched beyond the traditional in order to efficiently generate VLF band and below radio waves. [17] analyzed the possibility of using Deception Island in the Antarctic as a naturally occurring slot antenna. Field et al. have suggested and experimented with using a blimp to construct a monopole antenna for VLF radio operation [18]. At VLF, the vertical electric dipole suspended by the blimp exhibited a radiation efficiency greater than 90% but is difficult to deploy. [19] constructed a loop antenna over a mountain top achieving a radiated power efficiency of 200 μW/MW and a bandwidth of 0.02 Hz. However, the bandwidth makes the applications of this antenna limited.

1.4 Overview and Organization

This document proposes an electrically small antenna system which is inherently broadband. Results from a proof-of-concept system are presented, in which a 3-meter device transmits in the VLF radio band. The implications of such a device are widespread, and have applications to submarine communications, oil discovery, terrestrial radio navigation systems, and more [20–23]. The development of the broadband, efficient electrically short

transmitter featured in this paper is broken into the following chapters:

Chapter II explains the concept of operation. The purpose of this section will be to convince the reader that the theory of the system is mathematically sound, and grounded in physical principles. This section will abstract away the tools and instruments necessary to implement the system.

Chapter III provides the development milestones of the system. Fine details missing in the concept of operations are introduced in this section, and tool and instrument selection is explained. Technical specifications of the equipment used will be discussed, as well as the limitations that such equipment places on the system.

Chapter IV presents experimental results of the system. The Georgia Tech LF Lab AWESOME radio receiver is used to receive the radio signals transmitted by the featured system. The data is processed to show the broadband nature of the system at LF and below.

Finally, Chapter V contains the conclusion in which suggestions for future work are given.

CHAPTER 2

CONCEPT OF OPERATIONS

The operation of the system featured in this paper is best explained through transmission line theory. A transmission line is any medium that guides both voltage and current from one end to the other, such as a coaxial cable, but we discuss it here because antennas also have some properties that can explained in terms of transmission line theory. Transmission line theory is only relevant when the distance of the guiding medium is significant compared to a wavelength. An infinitesimally small section with length, dx, of the medium can be modeled as a two-port network, as seen in Figure 2.0.1.

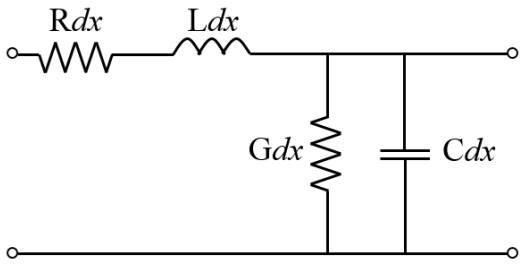

Figure 2.0.1: An infinitesimally small segment of transmission line.

From this model of a transmission line, the telegrapher's equations were formulated, which revolutionized the telegraphy industry in the early 1900's. The telegrapher's equations are seen in Equations 2.1 and 2.2, and predict how a wave will travel along a transmission line.

$$\frac{dV}{dx} = -L\frac{dI}{dt} - RI \tag{2.1}$$

$$\frac{dI}{dx} = -C\frac{dV}{dt} - GV \tag{2.2}$$

In these equations, L is the inductance per unit length, and C is capacitance per unit length. Both L and C impede, or slow down, the transfer of voltage and current from the left edge of the segment to the right edge of the segment, leading to a finite propagation delay.

The transmission line model can describe any such structure where a voltage and current waveform takes a non-zero amount of time to propagate through. For a transmission line, the phase velocity is given by

$$v_p = \frac{1}{\sqrt{LC}} \tag{2.3}$$

This equation states that the phase velocity of a wave is inversely proportional to the root of the product of the inductance and capacitance of the line per unit length. The presence of either slows the wave, and both must be non-zero in order for the wave propagation to not be instantaneous. Self-capacitance of a single metallic structure is realized through electric fields, whereas self-inductance is realized through magnetic fields. A single conductor in free space can be considered a two port network if the other conductor/port is taken to be at infinity. The self-capacitance and self-inductance therefore fits the model seen in Figure 2.0.1. For these reasons, an arbitrary metal conductor serving as an antenna can be approximated as a transmission line.

Transmission line theory can also be used to explain the input impedance of a conventional antenna. The intrinsic impedance of a transmission line is given by

$$Z_o = \sqrt{\frac{L}{C}} \tag{2.4}$$

and is the ratio of voltage to current for a waveform propagating along a transmission line. However, the intrinsic impedance is equivalent to the input impedance only if the transmission line is terminated to produce no reflections (or is infinite in length). In steady-state sinusoidal operation, reflections from transmission line discontinuities must be considered.

In these cases, the input impedance is simply stated as

$$Z_{in} = \frac{V^+ + V^-}{I^+ + I^-} \tag{2.5}$$

where the V^+, I^+ represent the forward going wave, and V^-, I^- represent the reflected wave at the feed.

2.1 Input Impedance of Conventional, Linear, and Time-Invariant Antennas

A conventional electric antenna can be approximated by a transmission line with an open circuit at the end. For a DC step-change voltage reaching the open circuit, the reflection coefficient, Γ_v = 1, while the current reflection coefficient is Γ_i = -1. The effects that the reflection coefficients have on input impedance and current are illustrated in Figure 2.1.1.

An incident current wave is launched onto the transmission line, denoted as I^+. The wave accrues a phase change of θ as it travels to the open circuit. Once at the open circuit, it reflects with a phase shift of π, which cancels the incident phasor at the open circuit. The phase of the reflected wave changes by an additional θ as it travels back to the source. At the source, the incident and reflected current waveforms add to produce the current at the input of the antenna. For electrically small antennas, θ is far less than π which causes the phasor at $z = 0$ in Figure 2.1.1 to nearly cancel the incident wave.

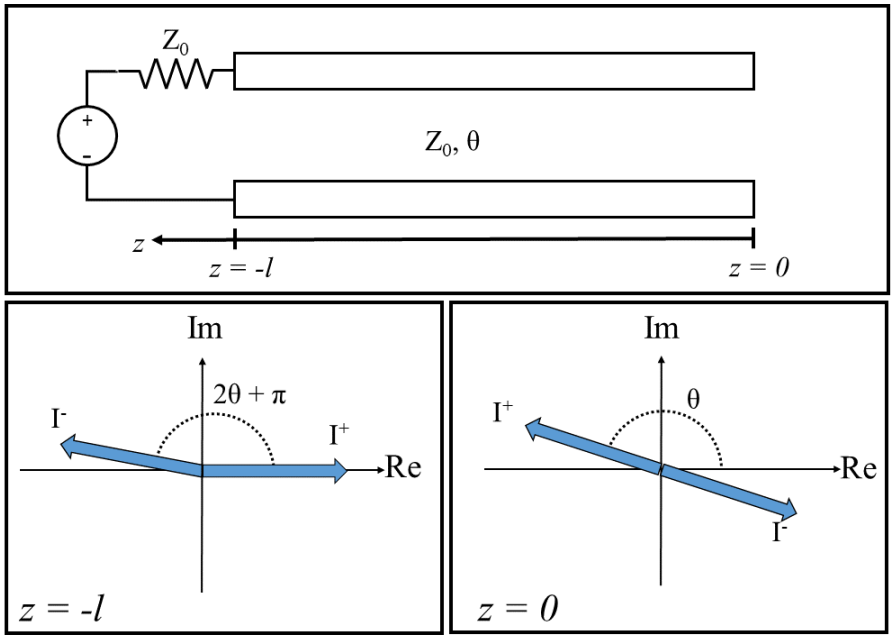

Figure 2.1.1: Phasor analysis of current on an open circuit transmission line.

Relating Figure 2.1.1 to Equation 2.5 is seen below for an electrically short antenna

$$Z_{in} = \frac{V^+ + V^+ e^{2j\theta}}{I^+ - I^+ e^{2j\theta}} \tag{2.6}$$

where the electrical length $\theta = \frac{l}{\lambda} \times 360°$. For an electrically small antenna, the denominator of Equation 2.6 is nearly zero.

The small quantity of current thus produces a large, reactive input impedance. The reflection from the open circuit is ultimately responsible for the issues associated with an ESA. Unlike that of an open circuit transmission line, a transmission line of infinite length has an input impedance of its intrinsic impedance. A goal of the system proposed in this document is to force an open circuit transmission line to behave like a transmission line of infinite length. This behavior is implemented in a number of steps, the first being discretizing a signal of interest with time-limited pulses.

2.2 Pulse Waveform Behavior on an Open Circuit Transmission Line

Consider a time-limited waveform injected onto a open circuit transmission line. This is classically analyzed through methods such as the bounce diagram as seen in Figure 2.2.1 . The pulse moves to the open circuit, and then reflects back to the source. In this case, a matched source is assumed and thus the pulse experiences only a single reflection.

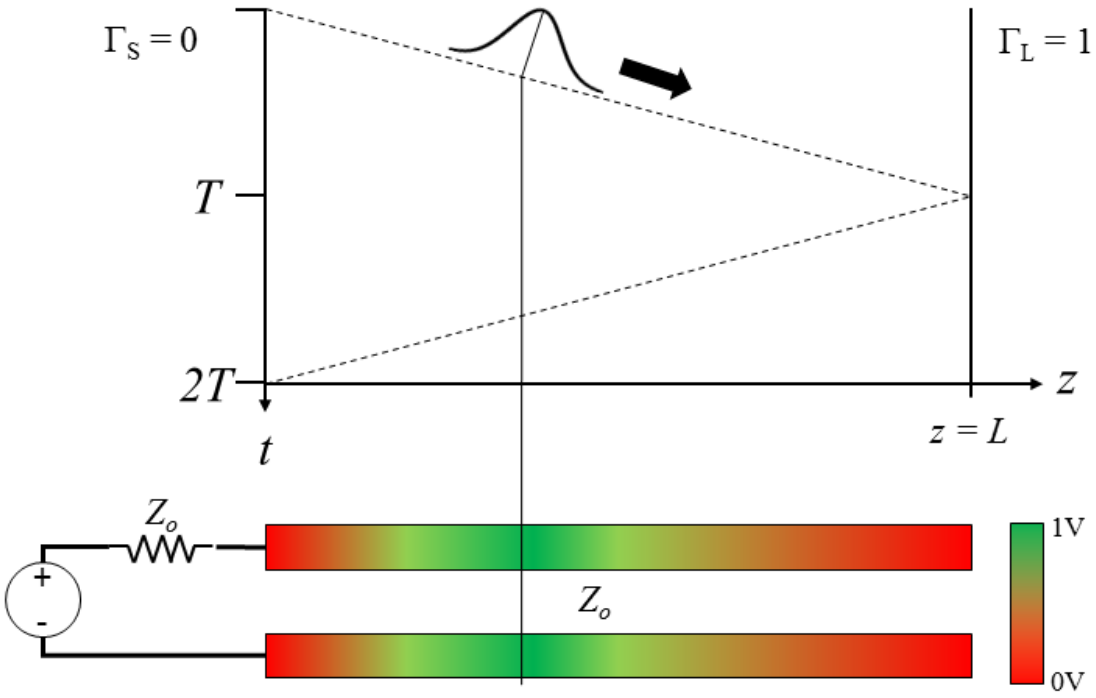

Figure 2.2.1: Bounce diagram illustrating the behavior of a pulse on an open circuit transmission line.

The novelty of this antenna system extrapolates on the concepts discussed above. Now consider introducing a switch into the transmission line, and opening the switch after the pulse has passed as illustrated in Figure 2.2.2. The pulse is trapped behind the switch, and therefore effectively matched to the intrinsic impedance of the transmission line.

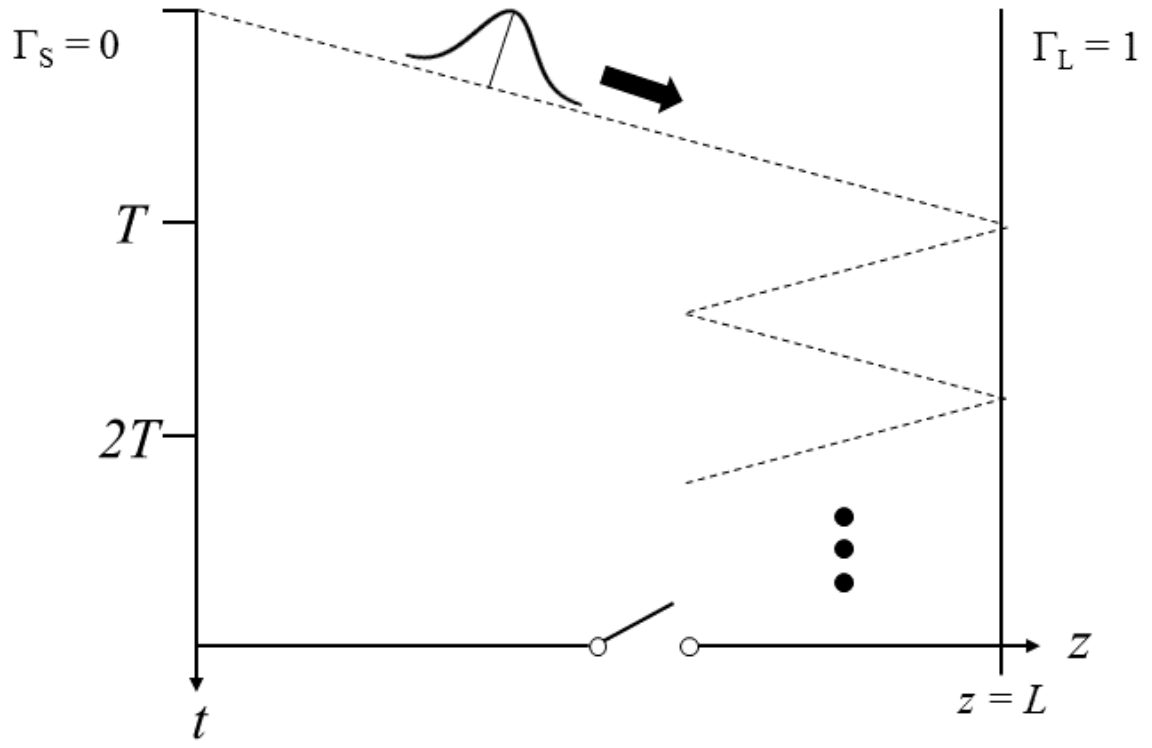

Figure 2.2.2: Bounce diagram illustrating the behavior of a pulse being trapped behind a switch.

2.3 Mixing Signal of Interest with Pulse Train

The applications of a single pulse are limited, however a pulse train finds much more utility. An arbitrary signal of interest can be mixed with a pulse train in order for desired information to be encoded, as seen in Figures 2.3.1 and 2.3.2. This allows the same concept seen in the above section to be applied repeatedly, where the switch is closed to allow a pulse into a storage region and opened to keep the pulse trapped.

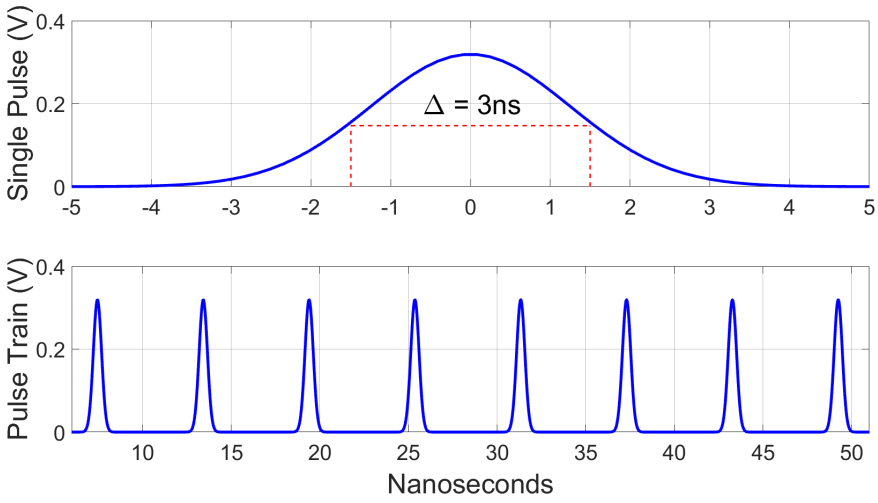

Figure 2.3.1: A single Gaussian voltage pulse and a Gaussian voltage pulse train as a function of time.

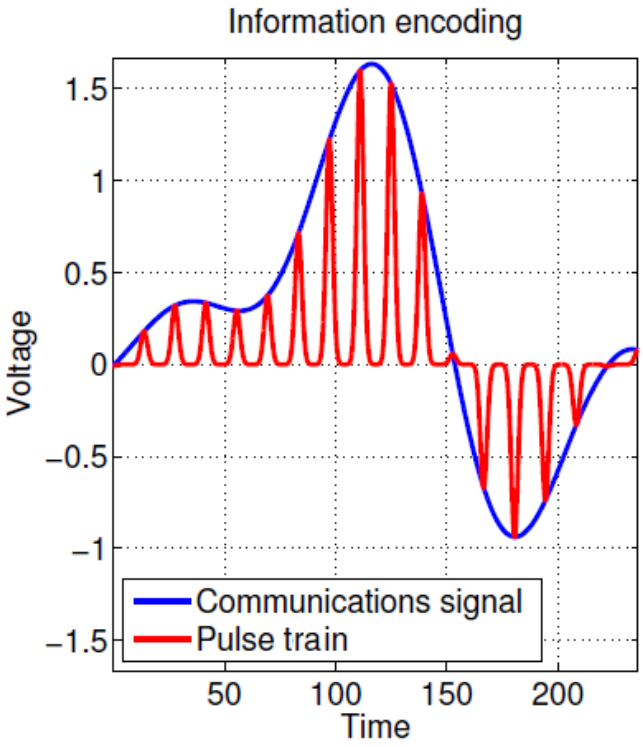

Figure 2.3.2: Arbitrary signal of interest mixed with a Gaussian pulse train. Courtesy M. Cohen.

2.4 Effects of Pulse Train Period on System Performance

The spectrum of a Gaussian pulse train can be seen in Figure 2.4.1. It can be seen that as the period shrinks, the spectrum approaches DC due to the frequency components widening to the edges of the Gaussian curve. Mixing a signal with DC does nothing to the signal, and is therefore considered to be an upper bound to the system's performance. A period comparable to 100ns produces significant and undesired frequency content in close proximity to DC (for T = 100ns, there is a spur in integer multiples of 10MHz). For periods greater than 100ns, the issue is worsened. When a signal is mixed and transmitted with a Gaussian pulse train of this period, there will be a large amount of noise spectrally close to the signal of interest, which could be transmitted, filtered, amplified, and received with the signal of interest. This is highly undesirable, and for successful operation this must be avoided. However, the pulse period is also determined by the RF switch speed and supporting circuitry, and underlines the importance of the technology for this application.

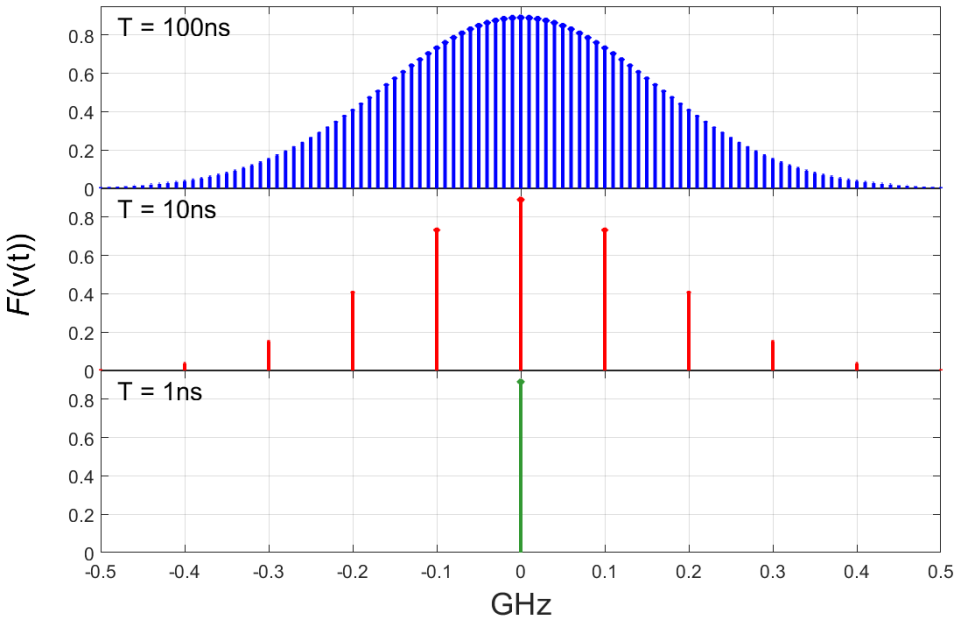

Figure 2.4.1: The spectrum of a Gaussian pulse train with a fixed duty cycle of 30% is seen for various periods.

Another consideration in selecting the pulse period is choosing the optimal period which minimizes the current allowed through the switch from the trapped region when it is closed. Due to physical limitations of RF switches, the switch will be held closed for a finite amount of time, which may allow trapped charge to return to the feed as illustrated in Figure 2.4.2. An optimal solution must take into account both the length and the velocity factor of the transmission line, as well as the switching speed of the switch.

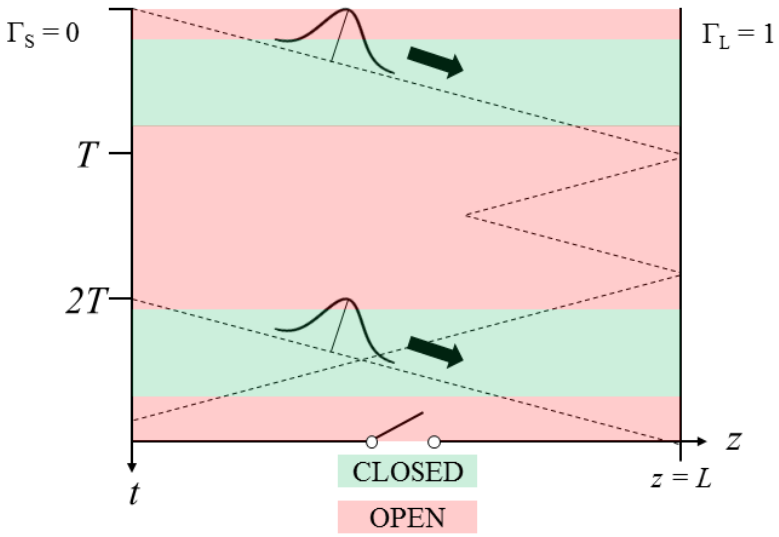

Figure 2.4.2: Bounce diagram depicting how a previously trapped pulse could be allowed back to the feed with poor timing.

CHAPTER 3

DEVELOPMENT MILESTONES

The development of a physical system that could implement the details found in Chapter 2 started with simple experiments and increased gradually in complexity. Two distinct phases of development were realized, and are recorded in this chapter.

3.1 Version 1.0 - Single Shot Pulse Trap

An early goal set for the project was to trap a single pulse in coaxial cable by closing and then opening a switch at the entrance, thus overcoming the first challenge of timing the switch with the arrival of a pulse. We accomplished this with commercial off-the-shelf parts. Figure 3.1.1 shows a block diagram of a system used to capture a single pulse behind an RF switch. Digital logic is used to trigger the switch at the appropriate time. In this experiment, 50 Ω coaxial cable is used throughout the system for simplicity. Cable A must be longer than the length of Cable B, but shorter than twice the length of Cable C for a pulse to be trapped. In this initial setup, nothing is radiating, the purpose is merely to achieve pulse trapping. Justifications for each portion seen in the block diagram are below.

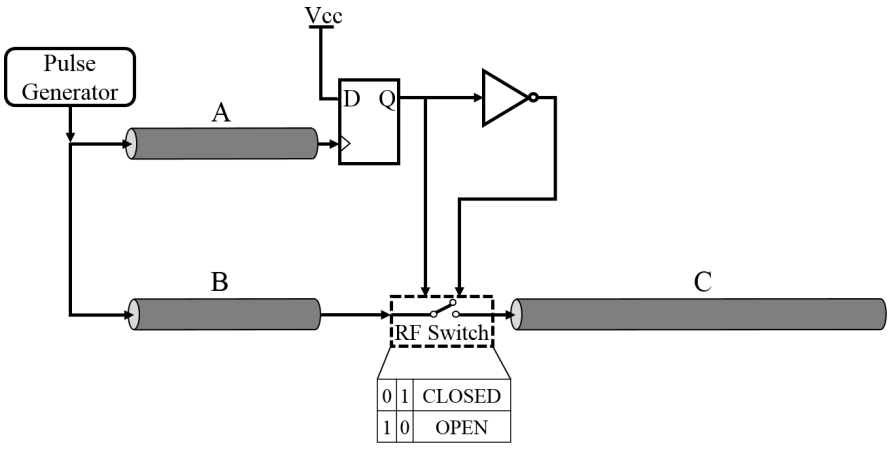

Figure 3.1.1: The first version of the system, which allows a single pulse to be trapped.

3.1.1 Pulse Generator

A signal source capable of generating a pulse train with a pulse width on the order of nanoseconds is needed for the system. The Berkeley Nucleonics Model 6040 was chosen, and as pictured in Figure 3.1.2. The Model 6040 can operate in single shot mode, or periodic mode with a repetition rate more than 20 MHz. Furthermore, the Model 6040 can produce pulses less than 5ns in duration into a 50 Ω load as shown in Figure 3.1.3.

Figure 3.1.2: The Berkeley Nucleonics Model 6040 is capable of providing impulse-like pulses to a 50 Ω load.

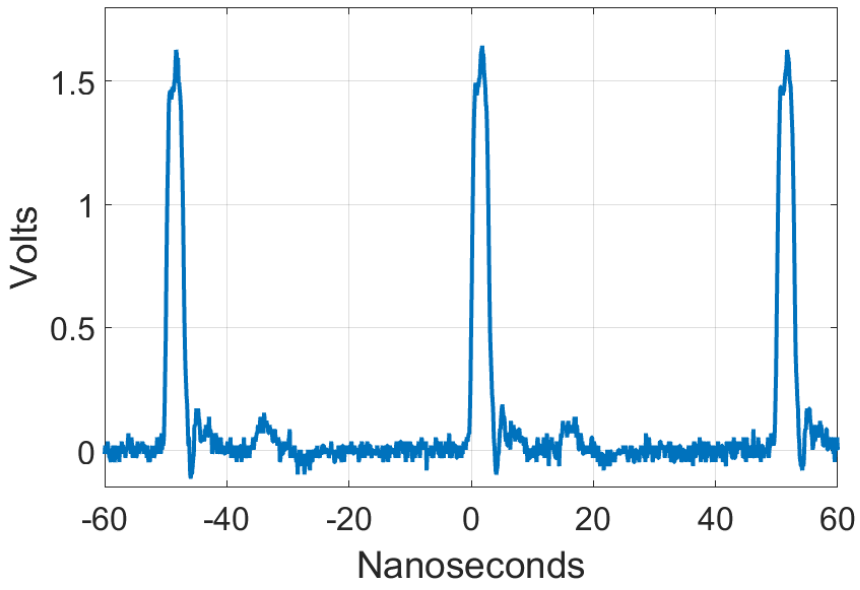

Figure 3.1.3: The plots above display a pulse train generated by the Berkeley Nucleonics Model 6040 terminated into a 50 Ω load.

3.1.2 RF Switch

The switching speed of the RF switch is critical to the performance of the system, as it must be able to go from closed to open faster than the pulse can propagate down cable C, reflect and return. At this stage, the switch is reflective instead of absorptive, so that little to no energy is returned through ground. An absorptive switch differs from a reflective switch because the unselected port is terminated with a 50 Ω resistor. The energy is therefore absorbed, hence the name. The unselected port of a reflective switch is simply an open circuit. After searching for a switch that would perform well based on these two merits, the Mini-Circuits RSW-2-25PA+ was chosen, and is pictured in Figure 3.1.4. The switching speed of the RSW-2-25PA+ is 14 nanoseconds, and has a nominal insertion loss of 1 dB at 1 GHz. No more than 1 watt of RF energy can be passed with this switch.

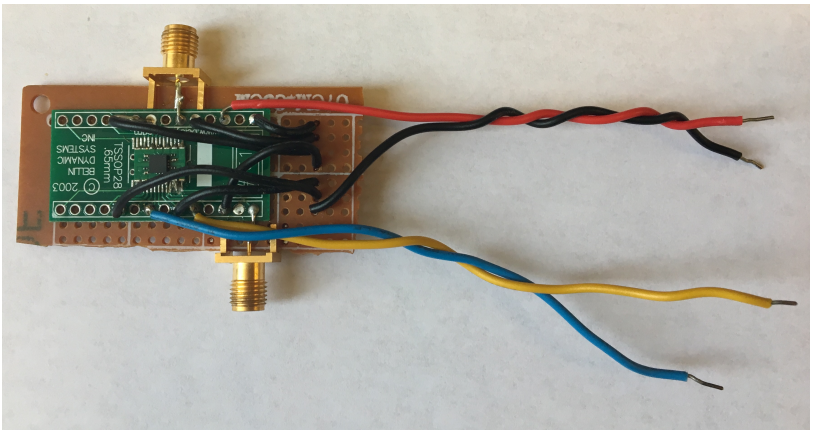

Figure 3.1.4: The Mini-Circuits RSW-2-25PA+ RF Switch as used in the first pulse trapping experiment.

This RF switch is controlled by two logic signals, as shown in Figure 3.1.1. A natural choice to control the switch is, therefore, a digital logic circuit.

3.1.3 Digital Logic and Timing

Due to the control signals of the RF switch requiring only 5V, the digital logic seen in Figure 3.1.1 was designed and assembled. The RF switch and the digital logic circuit were connected across a breadboard. Surface mount digital logic components were chosen in order to reduce propagation delay, and rise-fall time.

3.2 Single Shot Trapped Pulse Experiment

Using the Version 1.0 system detailed above, a pulse was trapped. Figure 3.2.1 displays the RF switch setup.

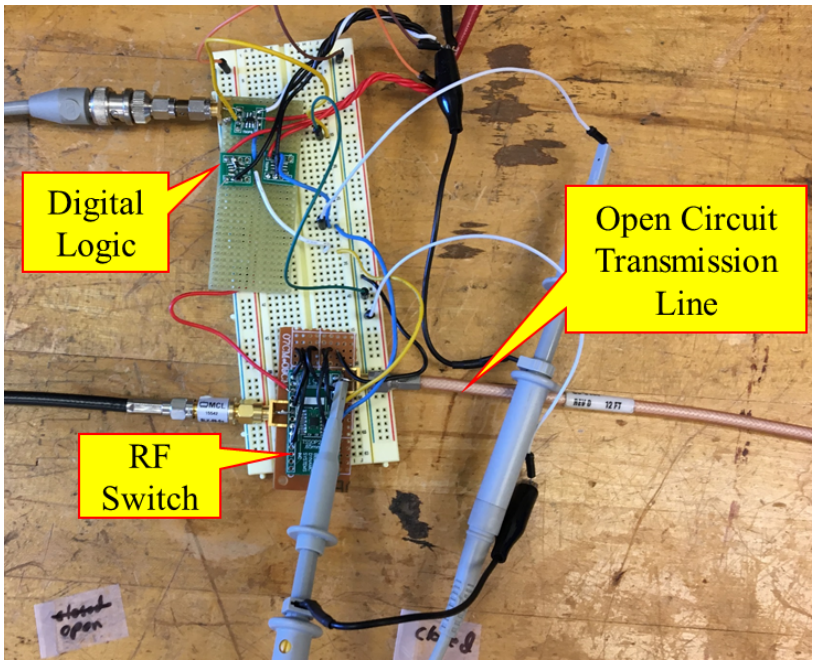

Figure 3.2.1: The setup used to trap a single pulse in an open circuit transmission line.

Several cases were probed during this experiment, resulting in Figures 3.2.3, 3.2.2, and 3.2.4. In these figures, the oscilloscope trace is color coded to match the probe location on the simplified block diagram. Figure 3.2.2 displays the case where the switch is held open, and the pulse can be seen to reflect off of the switch in this case. Figure 3.2.3 displays the case in which the switch is held closed. The pulse can be seen to strike the end of the transmission line and reflect. Figure 3.2.4 displays the case in which the switch is opened after the pulse has traversed the switch. The pulse can be seen bouncing in the charge storage region, and the open circuit transmission line has been effectively matched to the feed.

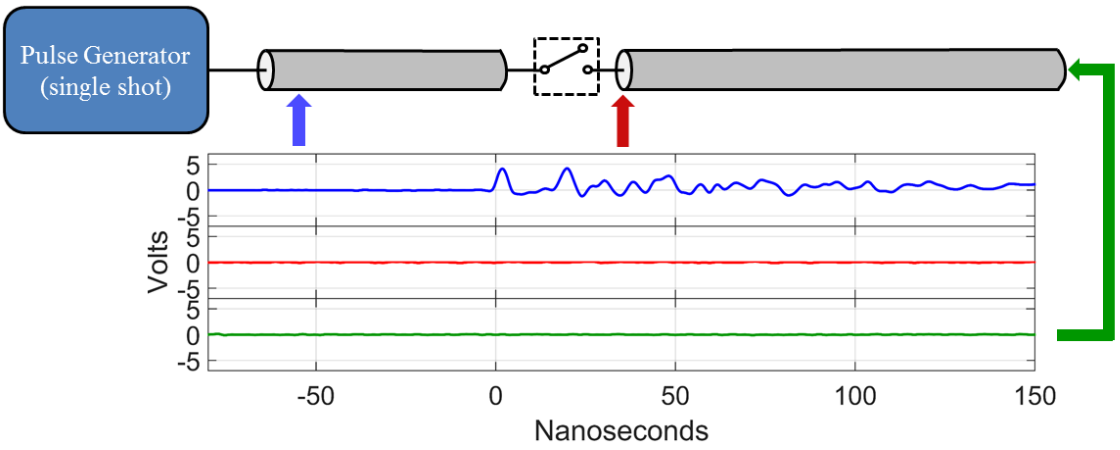

Figure 3.2.2: Oscilloscope traces with the switch set to remain open. The pulse reaches the switch and reflects.

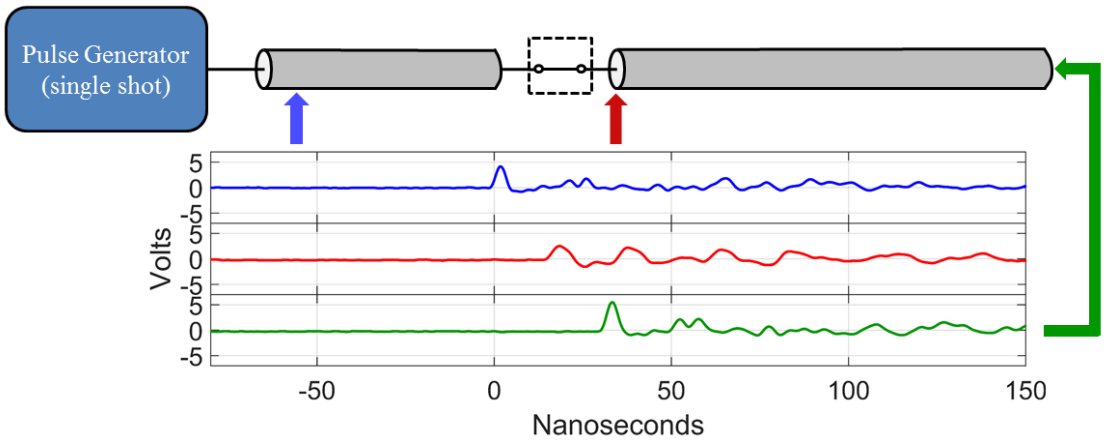

Figure 3.2.3: Oscilloscope traces with the switch set to remain closed. The pulse transmits through the RF switch, strikes the open circuit, and reflects.

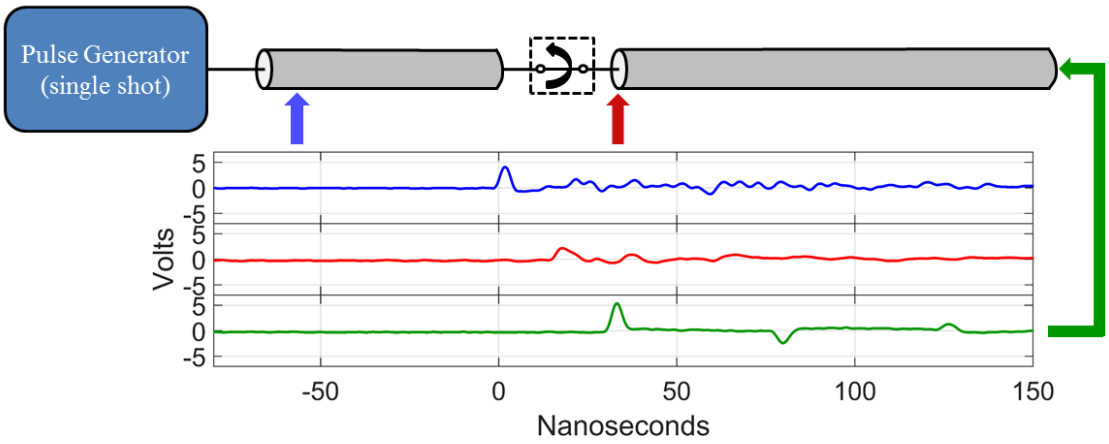

Figure 3.2.4: Oscilloscope traces with the switch set to start off closed, then open once the pulse has passed by. The pulse is trapped behind the switch, and bounces back and forth in the open circuit transmission line.

3.3 Version 2.0 - Repetitive Pulse Trapping and Adding Radiating Element

Having succeeded in trapping a pulse, we now aim to add a radiating element to the design so that the propagating current can generate electromagnetic waves. Figure 3.3.1 displays the block diagram of this implemented antenna system. Table 3.1 displays the upgrades made between the two versions.

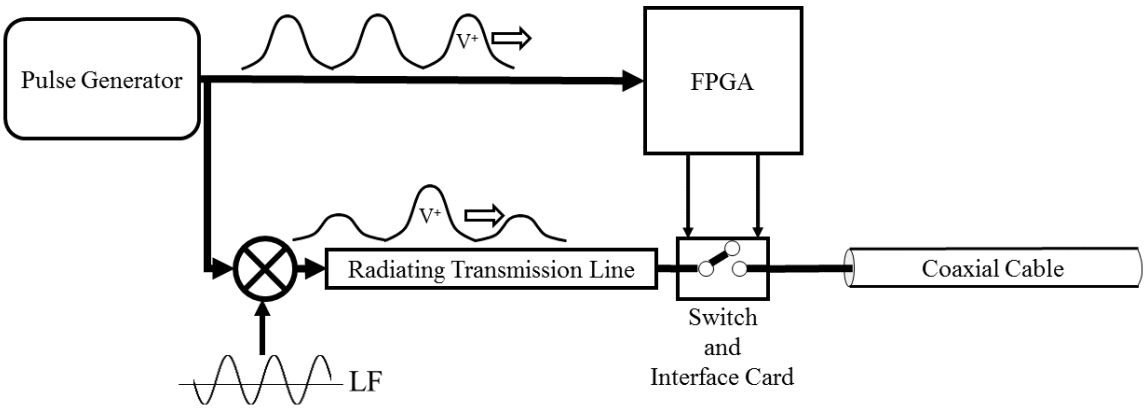

Figure 3.3.1: A complete block diagram of the antenna system.

Table 3.1: Upgrades made to Version 1.0 to implement Version 2.0.

Version 1.0	Version 2.0
No feedback in digital logic	Feedback in digital logic
Discrete Digital Logic	FPGA
Mini-Circuits RSW-2-25PA+ RF Switch	Mini-Circuits ZFSW-2-46 RF Switch
No Radiating Element	Single Conductor Transmission Line
No Modulation	Mini-Circuits ZAD-3+ Mixer

3.3.1 Digital Logic and Tuning

Field Programmable Gate Arrays (FPGAs) are commonly used for rapid prototyping of complex digital logic circuits, and are well suited to the needs of this project. The Altera Cyclone II was chosen due to its pervasiveness in academic classes. Figure 3.3.2 displays a block diagram with details of the digital logic circuit. The feedback in the digital logic circuit allows for the switch to be reset periodically.

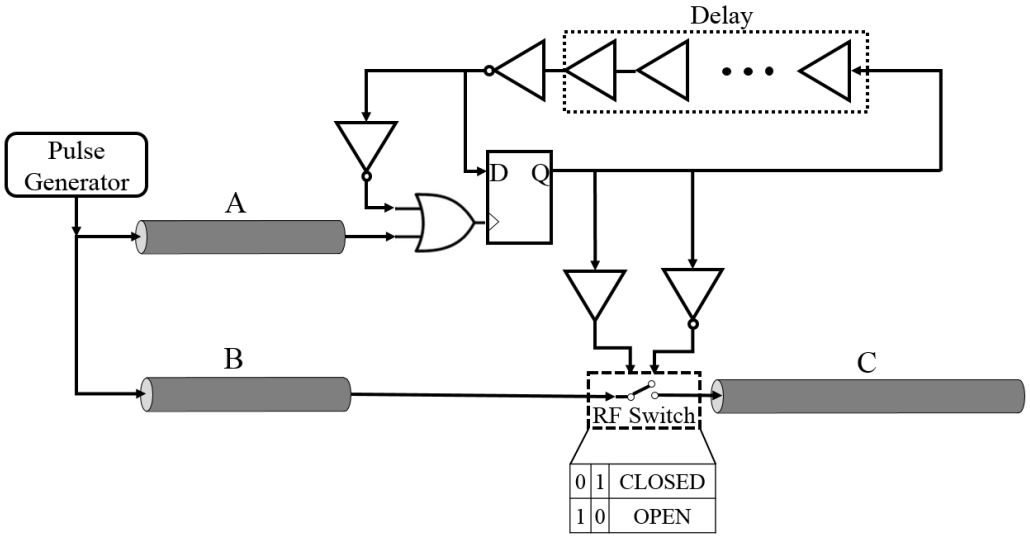

Figure 3.3.2: The second version allows for the switch to be reset periodically.

An FPGA provides the flexibility of adding delays into the circuit to increase the du-

ration of the gate-closed time, as well as precisely delaying the gate from opening. Figure 3.3.3 displays how the digital logic circuit can be modified with buffers, each with a delay of 0.36 nanoseconds, to tune the timing of the system.

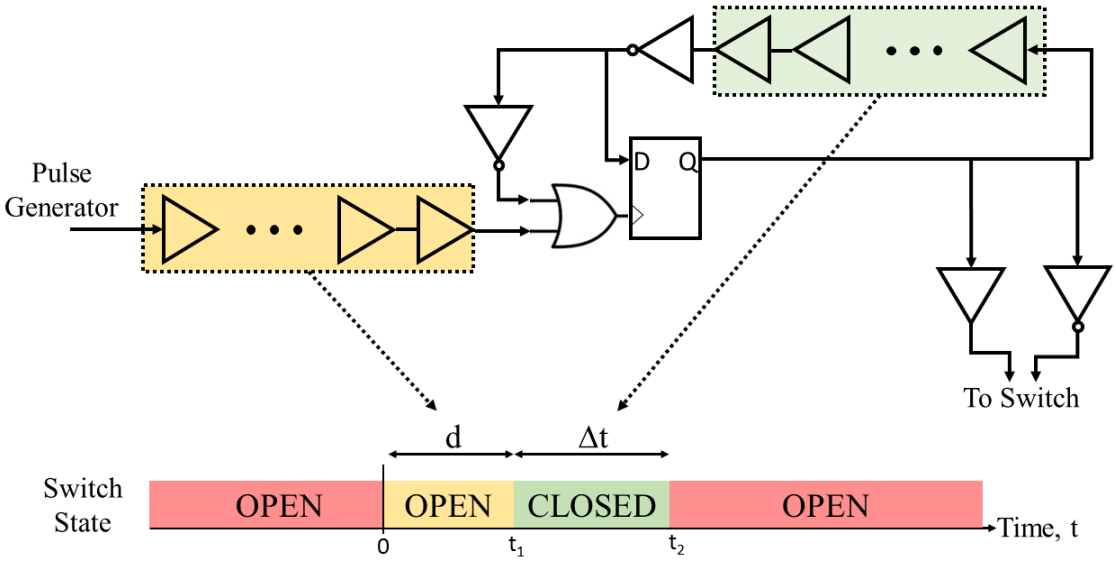

Figure 3.3.3: The buffers found in the digital logic allow for variable tuning of the switch.

Due to the possibility of altering the group delay of a component even slightly (e.g. using different cables), it is important to have a method by which to minutely adjust both the delay before the switch opens, and the duration of the interval in which the switch is closed. An oscilloscope with high-Z impedance is used to observe the waveform trapped behind the switch. A search is then performed to find the delays which maximize the energy stored behind the switch, as observed through the voltage amplitude on the oscilloscope.

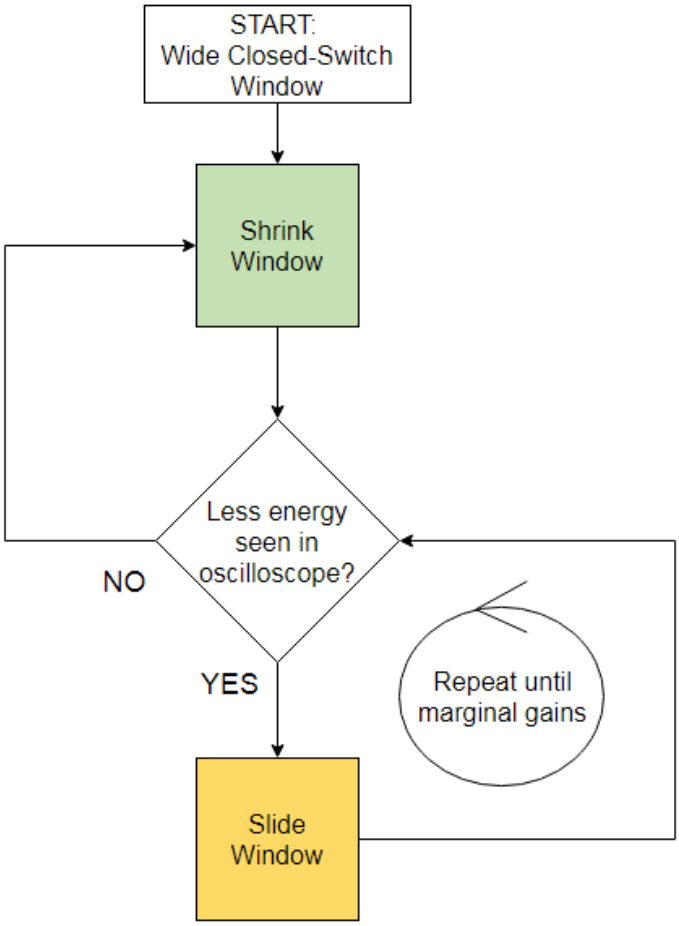

Figure 3.3.4: The steps to tune the system are seen above, where the blocks are color coded and correspond to the delays highlighted in Figure 3.3.3.

Figure 3.3.5 displays an oscilloscope trace of the tuning metric resulting from a poorly tuned circuit and a well tuned circuit. The end of the open circuit transmission line is probed with the high-Z input port of the oscilloscope, and the waveforms are observed. The poorly tuned window in red is due to the closed-switch window being too greatly delayed.

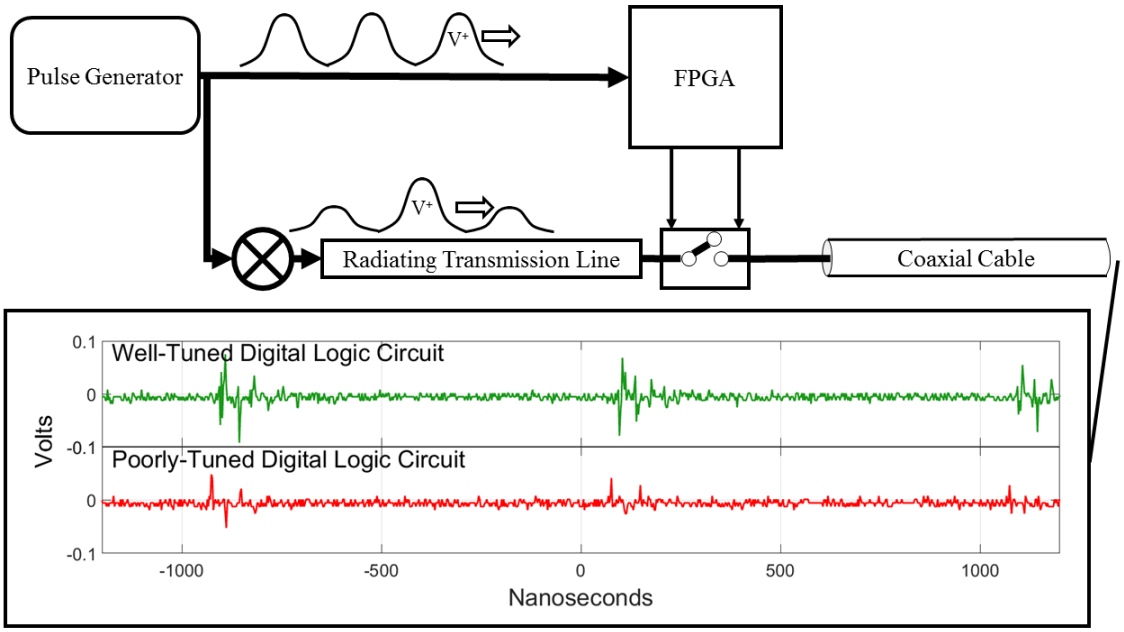

Figure 3.3.5: The end of the open circuit transmission line is probed with a high-Z port of the oscilloscope to produce the waveforms.

3.3.2 Interfacing with the RF Switch

Continued searching for an RF switch online resulted in the Mini-Circuits ZFSW-2-46 RF switch which has a switching speed of 4 nanoseconds. The faster switching speed allows for a great improvement in the system performance, however, comes at the price of a higher control voltage. In order to interface this switch with the FPGA, a custom printed circuit board was designed, ordered, and assembled. The ZFSW-2-46 RF switch requires a digital control signal where 0 and 1 correspond to 0V and -6V, respectively. In order to convert the 3.3V FPGA TTL signals to a signal capable of controlling a switch, an inverting amplifier topology is used with LM7171 operational amplifiers, as seen in Figure 3.3.6. The resulting signal level conversion can be seen in Figure 3.3.7.

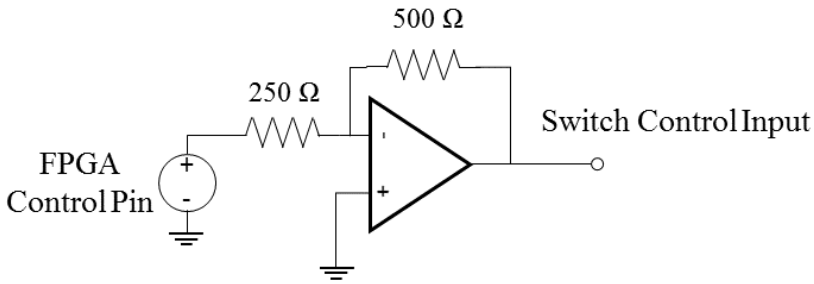

Figure 3.3.6: Schematic displaying the electronics used to interface the FPGA with the Mini-Circuits switch.

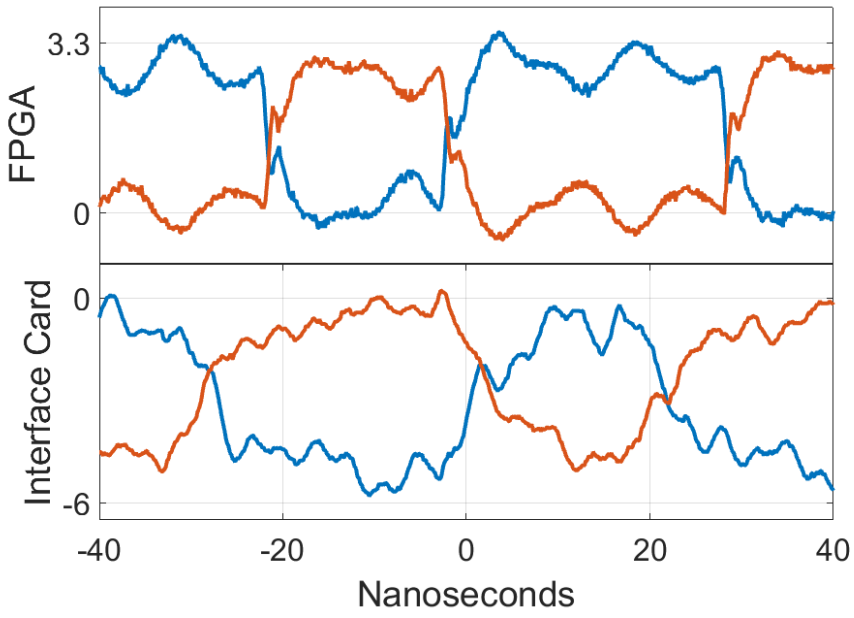

Figure 3.3.7: The FPGA control signal is transformed to be compatible with the RF switch, as seen above. These traces are taken from an oscilloscope.

After the FPGA to switch interface card was built, capacitors were added as needed to reduce oscillation of the operational amplifiers. In order to avoid bottlenecking the system, metrics such as slew rate were considered in the design of such a card. Figure 3.3.8 displays the full timing control of the system with annotations.

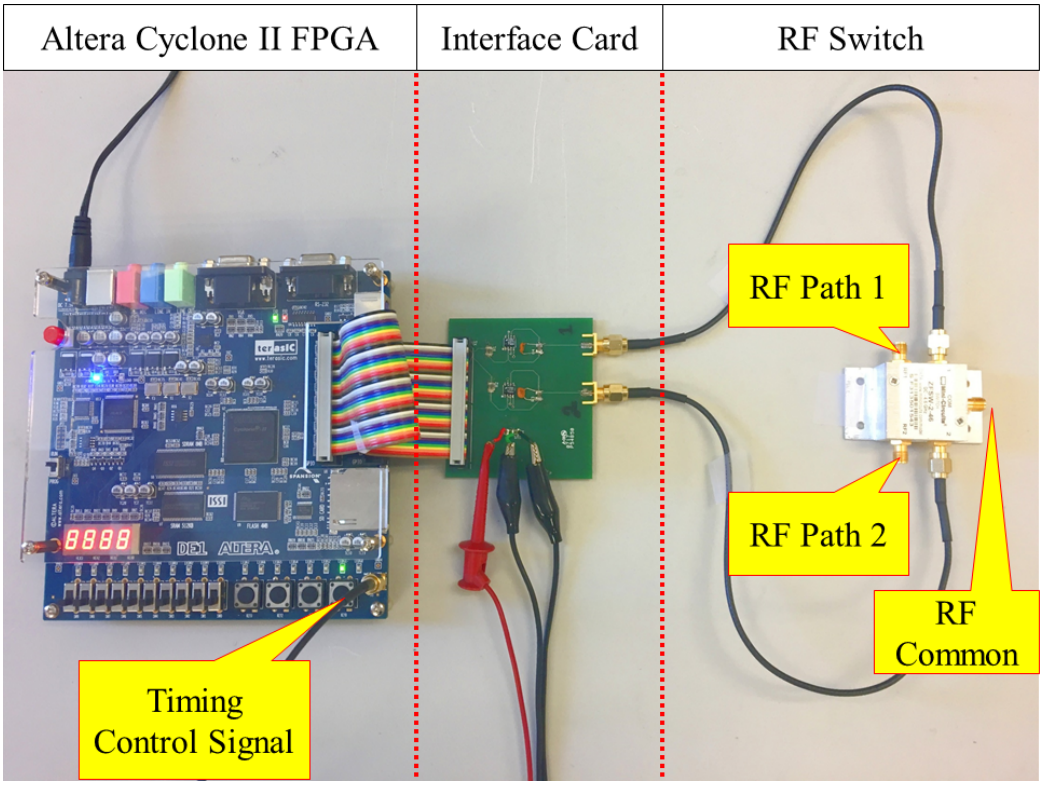

Figure 3.3.8: The timing system is annotated above for clarity.

3.3.3 Radiating Transmission Line

While transmission lines such as the coaxial cable are excellent for applications such as power transfer, they do not radiate. For functional operation, a component that both radiates and transmits energy from one port to another is desired. The difficulty of such a device is taking all desirable aspects from both a single port device and a two port device and combining them together. Ultimately, the sheath of a coaxial cable is what hinders it from radiating. Goubau [24] suggested that a single conductor transmission line is possible. From this source, such a device was fabricated in the lab, and is pictured in Figure 3.3.9. A diagram of the single conductor transmission line is picture in Figure 3.3.10. Figure 3.3.11 displays the cone used in the single conductor transmission line.

Figure 3.3.9: The single conductor transmission line used with the system.

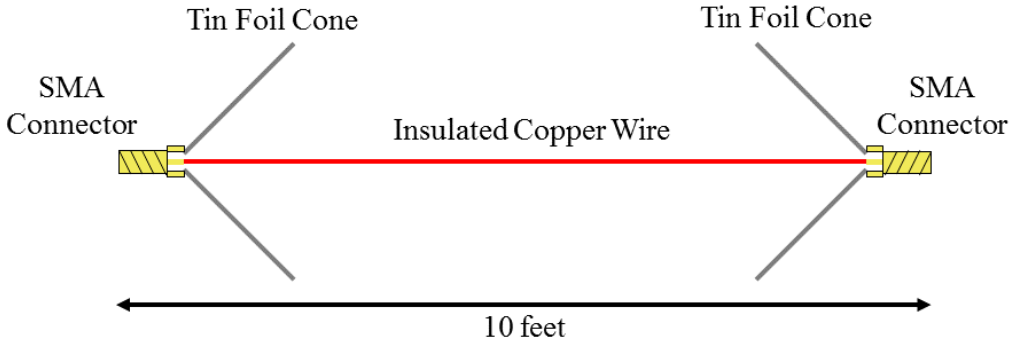

Figure 3.3.10: A diagram of the single conductor transmission line constructed for use in this system.

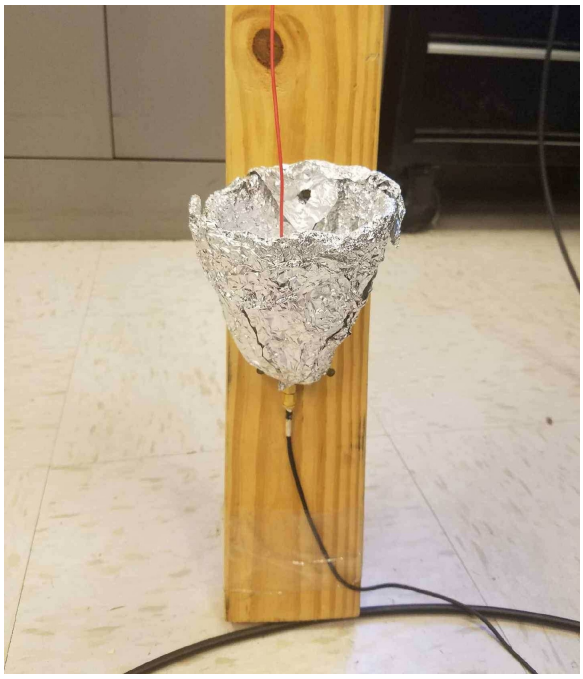

Figure 3.3.11: The coaxial cable to single wire interface is pictured above. The cone is approximately 11 inches in diameter at its widest point, and 11 inches tall.

The transfer function of the single conductor transmission line is computed by dividing the spectrum of an input and output pulse, as seen in Figure 3.3.12. The poor match of the single conductor transmission line means that the reflections from 50 Ω interfaces must be ignored in order to compute the transfer function. The waveform outside of the highlighted sections in Figure 3.3.12 are forced to zero in this calculation. The resulting transfer function is seen in Figure 3.3.13. The phase of the single conductor transmission line is found to be linear, and therefore does not cause dispersion. The single conductor transmission line does not conduct DC, however, does resonate at approximately 300 MHz.

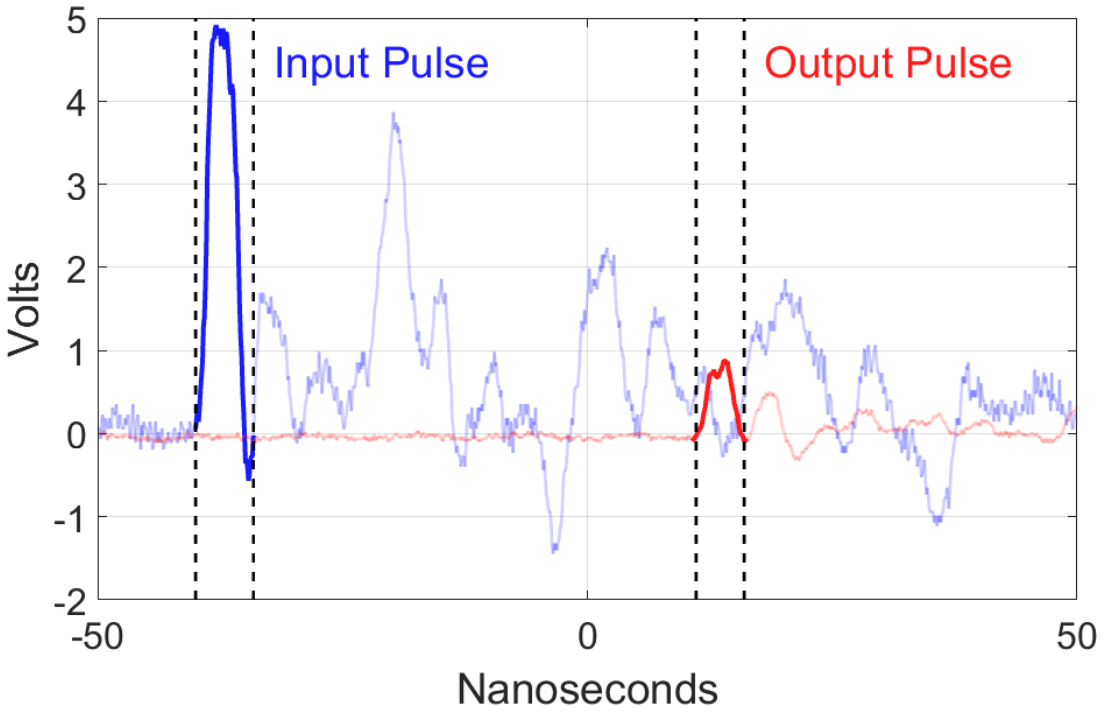

Figure 3.3.12: The reflections due to a mismatch to 50 Ω are not considered when calculating the transfer function.

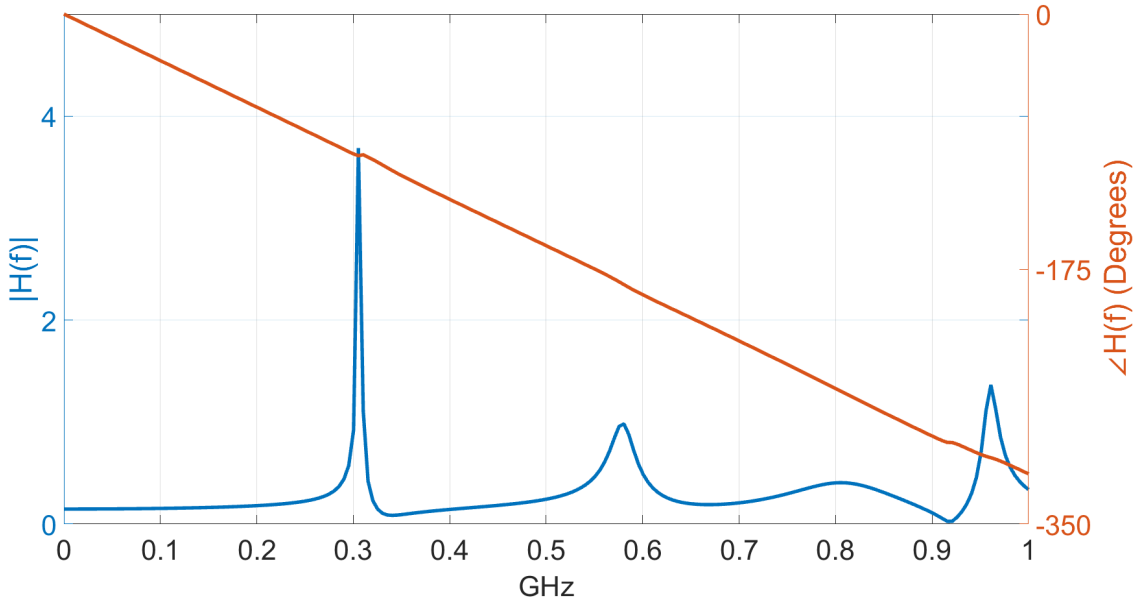

Figure 3.3.13: The transfer function of the single conductor transmission line used in the system.

The numerical electromagnetic simulations program 4NEC is used to model and simulate the input impedance of the single conductor transmission line. The model is pictured

in Figure 3.3.14. The simulated reflection coefficient is seen in Figure 3.3.15. The large reflections will have an adverse effect on the system performance.

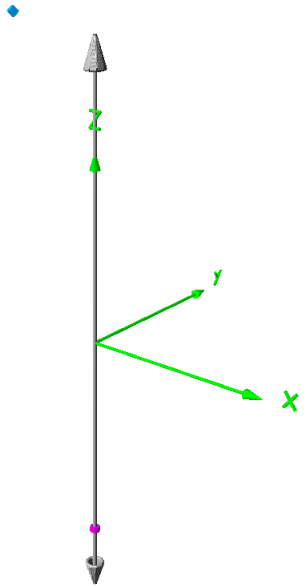

Figure 3.3.14: The single conductor transmission line modeled in 4NEC.

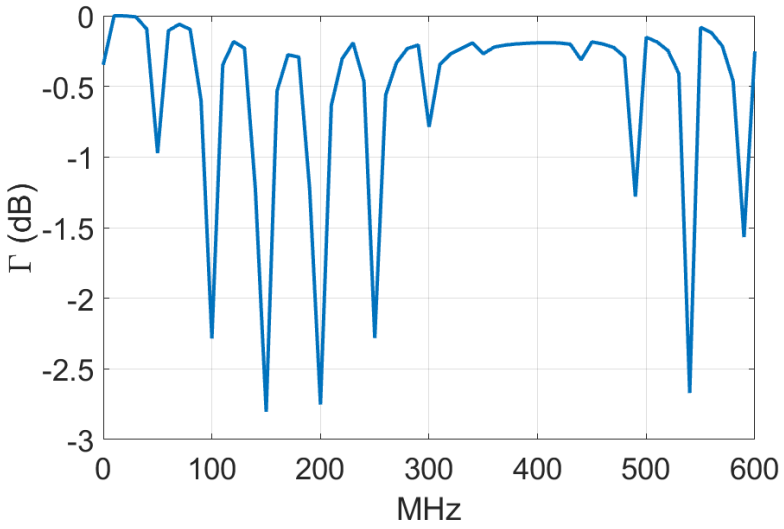

Figure 3.3.15: Simulated reflection coefficient in dB when using the single conductor transmission line with a 50 Ω system.

3.3.4 Mixing

Version 2.0 includes the ability of modulating a signal of interest with a pulse train. This is accomplished through the Mini-Circuits ZAD-3+ mixer, which is capable of mixing signals from 25kHz to 200MHz. Figure 3.3.16 displays a 30kHz sinusoid mixed with a pulse train with a period of 50 nanoseconds and a pulse width of 3 nanoseconds. The mixer effectively discretizes the continuous signal of interest.

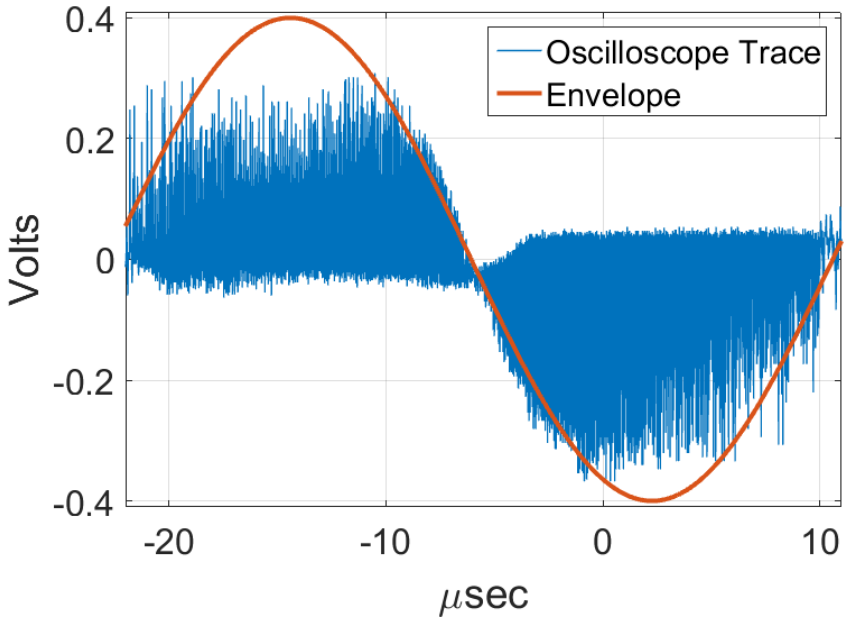

Figure 3.3.16: A pulse train modulated 30kHz sine wave produced by the mixer into a 50 Ω load.

CHAPTER 4

FULL SCALE TESTING AND RESULTS

The Georgia Tech Low Frequency Radio Lab has developed sensitive low frequency radio receivers which are capable of detecting magnetic fields weaker than 1 femtotesla. Using these receivers, radio signals transmitted by the novel antenna system can be detected. Figure 4.0.1 displays the setup used to measure the field strength generated by the antenna system. The Georgia Tech AWESOME LF Receiver is pictured in Figure 4.0.2. A magnetic loop air-core antenna commonly deployed with the receiver is shown in Figure 4.0.3. The full system is pictured in Figure 4.0.4 on the roof the Georgia Tech Van Leer building.

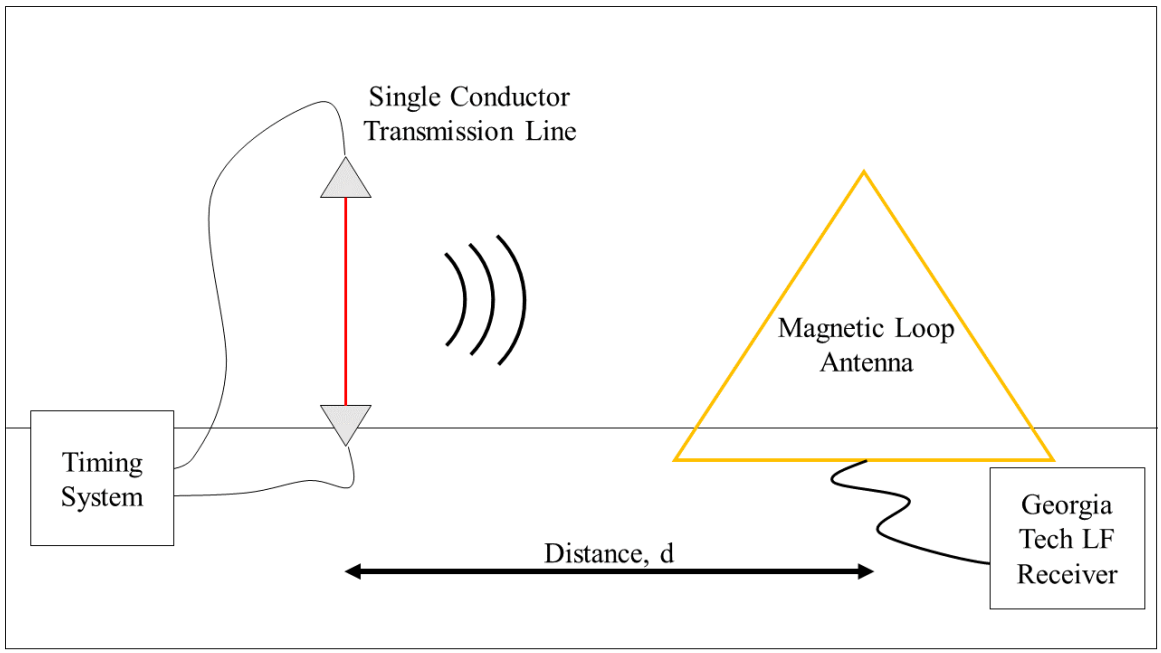

Figure 4.0.1: The experiments are conducted as seen in the diagram above.

Figure 4.0.2: The Georgia Tech AWESOME LF receiver is pictured above. Courtesy M. Cohen.

Figure 4.0.3: Pictured above is a magnetic loop antenna used by the Georgia Tech AWESOME LF receiver seen in Figure 4.0.2. Courtesy M. Cohen.

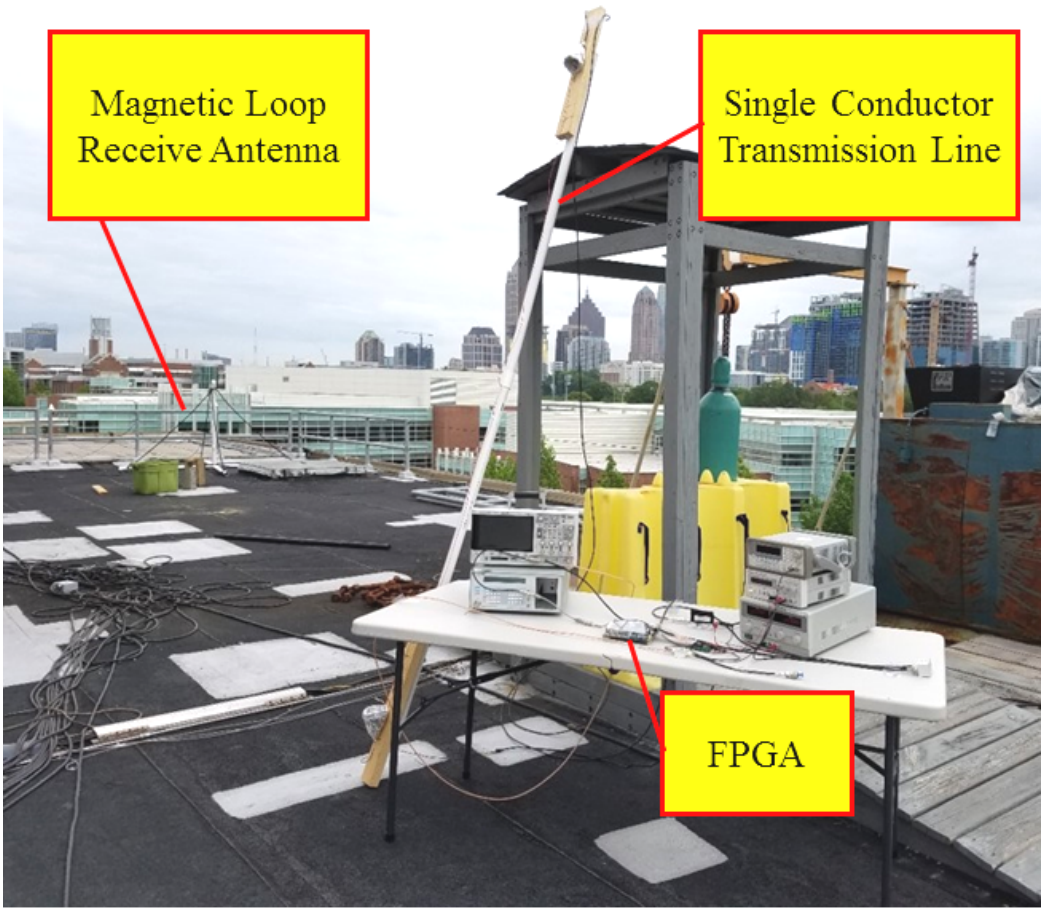

Figure 4.0.4: Preliminary tests occurred on the roof of the Georgia Tech Van Leer building.

4.1 Objectives

The experiments detailed in this chapter demonstrate that the novel antenna system:

1. outperforms a conventional whip antenna of the same size in radiated power
2. is broadband in the LF and below radio bands.

4.1.1 Radiation Comparison with Whip Antenna

It should be noted that the system we have built is not fully optimized, in large part because of the reflection at the cones that convert the coaxial cable signal to the radiating wire, and back again. So in essence this prototype is 90% conventional antenna, and 10%

reflection suppressed antenna. Nonetheless, given the orders of magnitude improvement we expect for such electrically short antennas, the factor of 10 reduction should be more than compensated for. Hence, the system detailed in this document should far exceed the performance of conventional antennas due to the suppression of reflections as described in Chapter 2. For a more controlled experiment, the system can be modified to effectively operate as a whip antenna by holding the switch in a fixed state. Results gathered compare the case when switching is active versus when the system is operated as a whip antenna.

4.1.2 Bandwidth Limits

According to theory, the antenna system should not exhibit high Q in the LF radio bands and below. This theory can be confirmed by using a chirp as the signal of interest to the novel antenna system.

4.2 Results

The following plots display results taken from field tests with the novel antenna system described in this paper. Due to the noisy radio environment in Atlanta, the following results were taken at the Charlie-Elliot Wildlife Center in Mansfield, GA. The first figure displays the spectrum of the magnetic field for a conventional whip antenna and the novel antenna system. It can be seen that the novel antenna system produces a magnetic field which exceeds that of the conventional antenna by over 20dB. Figure 4.2.1 was taken at a distance of approximately 25 meters from the single conductor transmission line.

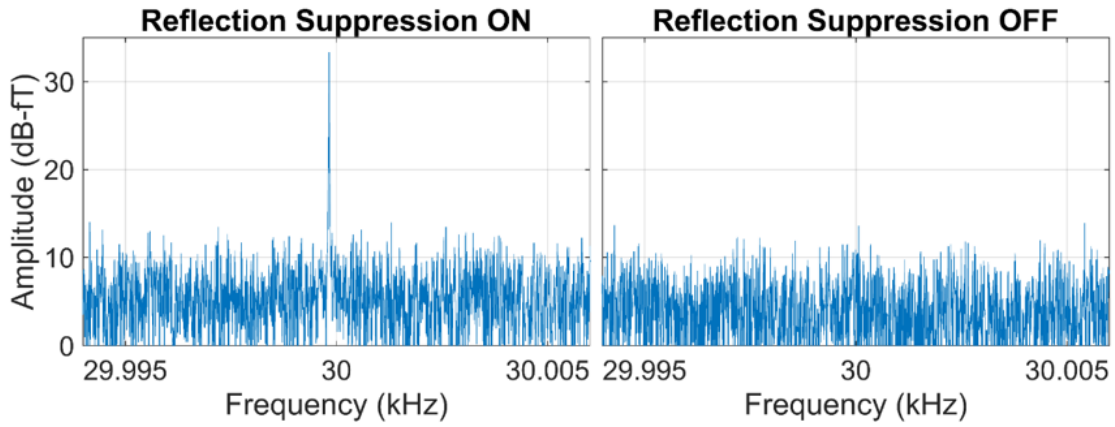

Figure 4.2.1: Significant increase in radiated power is observed when an effort is made to suppress the reflections. These measurements were taken at a distance of 25 meters. Courtesy M. Cohen.

Spectrograms allow for a time-frequency analysis of a signal of interest. Figure 4.2.2 displays a spectrogram of the received magnetic field. A chirp was used as the input to the novel antenna system. The reader should notice that the chirp is received, and the coefficients do not exhibit sharp resonance as with antennas in steady-state sinusoidal operation.

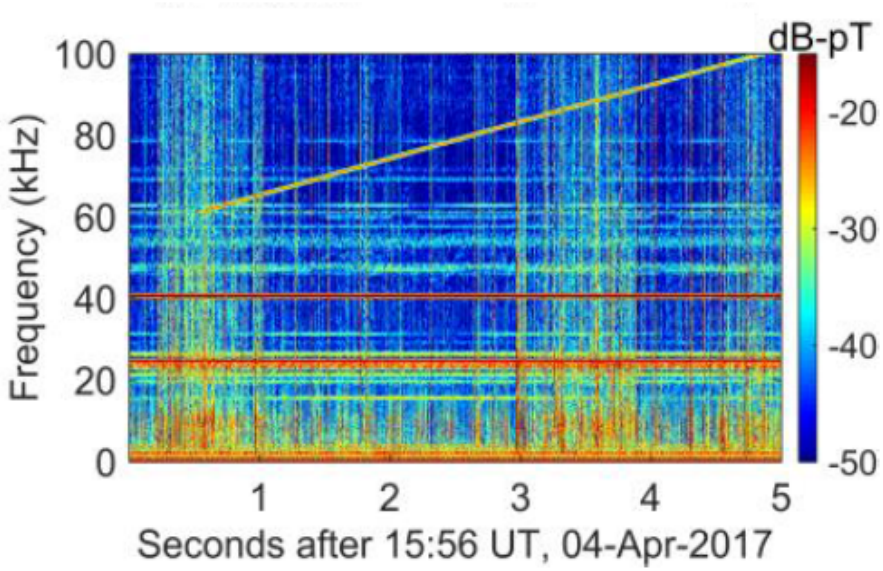

Figure 4.2.2: The broadband nature of the antenna system is shown in the spectrogram. Courtesy M. Cohen.

CHAPTER 5
CONCLUSION

A novel antenna system with time-varying properties which allows for efficient radiation in the LF radio band has been presented in this document. The development process is outlined, and the experimental results are documented.

5.1 Suggestions for Future Work

Admittedly, the system described herein is lacking due to using commercial off the shelf parts and bending them to fit our purposes. The issues that the system faces are ranked below:

- The single conductor transmission line has a poor match to the 50 Ω system
- The Mini-Circuits ZAD-3+ mixer causes ringing when a pulse is incident
- The switching speed of the Mini-Circuits ZFSW-2-46 RF switch is slow
- The Mini-Circuits ZFSW-2-46 RF switch is only suited for low power applications.

5.1.1 Matching the Single Conductor Transmission Line

The fabrication of the single conductor transmission line was based purely on [24]. This source made no mention of scattering parameters, or other relevant metrics for RF applications. Simulation mentioned previously in this thesis allows for a better design of a single conductor transmission line. Parameters such as cone pitch, cone length, and center conductor width can be varied to produce a better match to 50 Ω.

5.1.2 Replacing the Mixer

The mixer currently used in the setup reflects a significant portion of each pulse it receives. This causes ringing between the pulse generator and the mixer which effectively widens the waveform due to repeated mixing of the reflected pulse. An example of this action is shown in Figure 5.1.1.

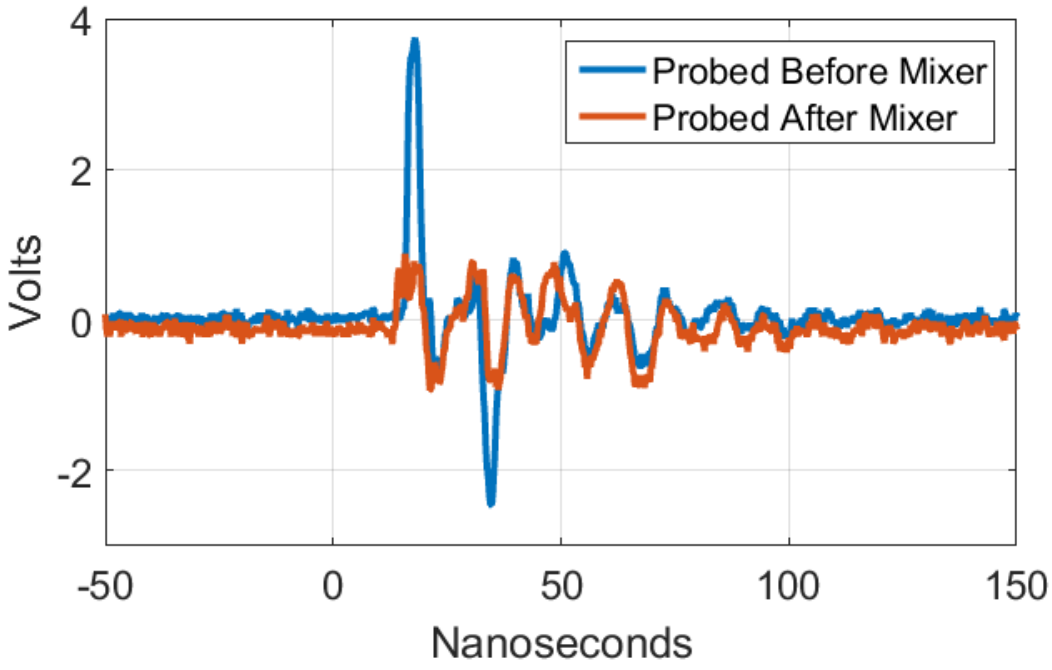

Figure 5.1.1: The waveforms probed before and after the mixer with an oscilloscope have been time-aligned to display that each reflection is mixed.

For the purposes of discretizing a continuous time waveform into a series of pulses, an absorptive switch can serve the same purpose. Furthermore, the hardware necessary to control such a switch at these time-scales has already been developed and implemented. For these reasons, future version of the novel antenna system will use an absorptive switch to modulate the signal of interest. Figure 5.1.2 displays a diagram showing how the concept will work.

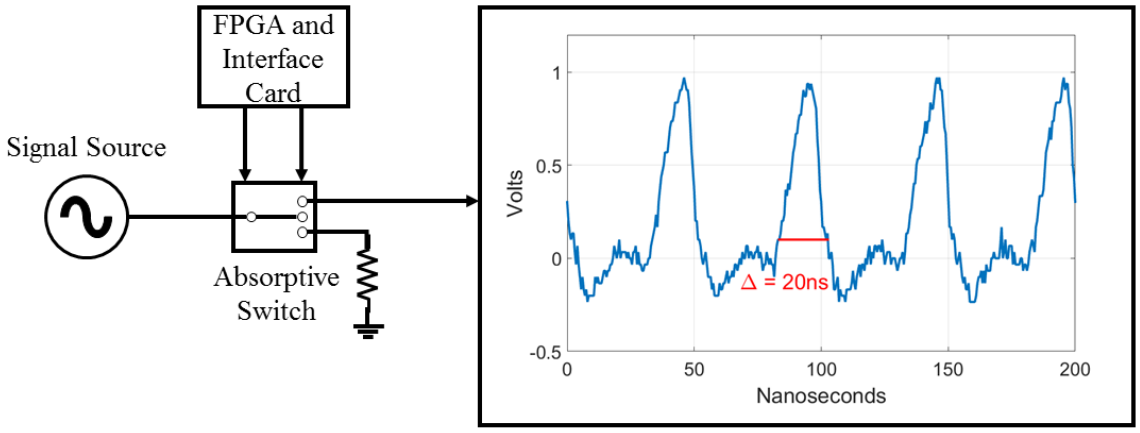

Figure 5.1.2: An absorptive switch can be used to the same effect as mixing a pulse train with a signal of interest.

5.1.3 Improvements in RF Switch

The theory found in Chapter 2 suggests that pulse train period fundamentally limits signal integrity, as seen in Figure 2.4.1. The pulse train period is determined by the time it takes for the RF switch to transition from a closed position to an open position. While other components mentioned previously will affect the efficiency of the system, the switching speed introduces non-linear effects that will corrupt the signal instead of simply attenuating it. For these reasons, developing a higher speed switch capable of handling more power is of great interest. Recent advances in semiconductor technology have produced the gallium nitride transistor, which promises both higher power and switching speeds [25]. Future versions of the novel antenna system will use this technology in RF switches for higher power operation of the system.

BIBLIOGRAPHY

[1] TriData Corporation, "NIOSH Firefighter Radio Communications," Sep. 2003.

[2] D. D. Crombie, "On the use of vlf measurements for obtaining information on the lower ionosphere (especially during solar flares)," *Proceedings of the IEEE*, vol. 45, no. 1/2, pp. 2027 –2034, 1975.

[3] B. Burgess and T. B. Jones, "The propagation of l.f. and v.l.f. radio waves with reference to some systems applications," *The Radio and Electronic Engineer*, vol. 45, no. 1/2, pp. 47 –61, Jan. 1975.

[4] S. L. Bernstein *et al.*, "Long-range communications at extremely low frequencies," *Proceedings of the IEEE*, vol. 62, no. 3, pp. 292 –312, Mar. 1974.

[5] R. Barr *et al.*, "Elf and vlf radio waves," *Journal of Atmospheric and Solar-Terrestrial Physics*, vol. 62, pp. 1689 –1718, 2000.

[6] M. B. Cohen *et al.*, "Broadband VLF/LF/MF Radio Reception and Remote Sensing with the AWESOME Instrument," *IEEE Transactions on Geoscience and Remote Sensing*, to be published.

[7] K. G. Budden, *Radio Waves in the Ionosphere, The Mathematical Theory of the Reflection of Radio Waves from Stratified Ionised Layers*. 1961.

[8] L. J. Chu, "Physical Limitations of Omni-Directional Antennas," *Journal of Applied Physics*, vol. 19, p. 1163, May 1948.

[9] R. F. Harringtion, "Effect of Antenna Size on Gain, Bandwidth, and Efficiency," *Journal of Research of the Nation Bureau of Standards*, vol. 64D, pp. 1–11, 1960.

[10] R. C. Fenwick, "A New Class of Electrically Small Antennas," *IEEE Transactions on Antennas and Propagation*, pp. 379–383, May 1965.

[11] R. M. Fano, "Theoretical Limitations on the Broadband Matching of Arbitrary Impedances," *MIT Technical Report*, vol. 41, Jan. 1950.

[12] D. F. Schwartz and J. C. Allen, "Wide-Band Impedance Matching: H-infinity Performance Bounds," *IEEE Transactions on Circuits and Systems - II: Express Briefs*, vol. 51, no. 7, pp. 364–368, Jul. 2004.

[13] S. E. Sussman-Fort and R. M. Rudish, "Non-Foster Impedance Matching of Electrically-Small Antennas," *IEEE Transactions on Antennas and Propagation*, vol. 57, no. 8, pp. 2230–2241, Aug. 2009.

[14] R. W. Ziolkowski and A. Erentok, "Metamaterial-Based Efficient Electrically Small Antennas," *IEEE Transactions on Antennas and Propagation*, vol. 54, no. 7, pp. 2113–2130, Jul. 2006.

[15] W. Yao and Y. Wang, "Direct Antenna Modulation - A Promise for Ultra-Wideband (UWB) Transmitting," *IEEE MTT-S Digest*, pp. 1273–1276, 2004.

[16] Watt, *V.L.F Radio Engineering*. Pergamon Press, 1967.

[17] M. G. Morgan, "An island as a natural very-low-frequency transmitting antenna," *IRE Transactions on Antennas and Propagation*, pp. 528 –530, Sep. 1960.

[18] E. C. Field *et al.*, "An aerostat-supported ELF/VLF transmitter," *Radio Science*, vol. 24, no. 2, pp. 235–246, Mar. 1989.

[19] R. Barr *et al.*, "Elf, vlf, and lf radiation from a very large loop antenna with a mountain core," *IRE Proceedings-H*, vol. 140, no. 2, pp. 129 –134, Apr. 1993.

[20] D. F. Rivera and R. Bansal, "Towed Antennas for US Submarine Communications: A Historical Perspective," *IEEE Antennas and Propagation Magazine*, vol. 46, no. 1, pp. 23–36, Feb. 2004.

[21] J. J. Simpson *et al.*, "FDTD Modeling of a Novel ELF Radar for Major Oil Deposits Using a Three-Dimensional Geodesic Grid of the Earth-Ionosphere Waveguide," *IEEE Transactions on Antennas and Propagation*, vol. 54, no. 6, pp. 1734–1741, Jun. 2006.

[22] J. H. Blakey, "Navigating Towards the Future: Transitioning From Terrestrial Radio Navigation to Satellite Navigation and Airborne Surveillance," *IEEE A & E Systems Magazine*, pp. 17–21, May 2006.

[23] M. B. Cohen *et al.*, "Sensitive Broadband ELF/VLF Radio Reception With the AWESOME Instrument," *IEEE Transactions on Geoscience and Remote Sensing*, vol. 48, no. 1, pp. 3–17, Jan. 2010.

[24] G. Goubau, "Single-Conductor Surface-Wave Transmission Lines," *Proceedings of the I.R.E*, pp. 619–623, Jun. 1951.

[25] K. S. Boutros *et al.*, "GaN Power Electronics for Automotive Applications," *IEEE Energytech*, May 2012.